Langmuir

Article

pubs.acs.org/Langmuir

# Investigation into the Formation and Adhesion of Cyclopentane Hydrates on Mechanically Robust Vapor-Deposited Polymeric Coatings

Hossein Sojoudi,[†,‡] Matthew R. Walsh,[§] Karen K. Gleason,*[,†] and Gareth H. McKinley*[,‡]

[†]Department of Chemical Engineering and [‡]Department of Mechanical Engineering, Massachusetts Institute of Technology, 77 Massachusetts Avenue, Cambridge, Massachusetts 02139, United States

[§]Chevron Energy Technology Company, Flow Assurance, 1200 Smith Street, Houston, Texas 77002, United States

Supporting Information

**ABSTRACT:** Blockage of pipelines by formation and accumulation of clathrate hydrates of natural gases (also called gas hydrates) can compromise project safety and economics in oil and gas operations, particularly at high pressures and low temperatures such as those found in subsea or arctic environments. Cyclopentane (CyC5) hydrate has attracted interest as a model system for studying natural gas hydrates, because CyC5, like typical natural gas hydrate formers, is almost fully immiscible in water; and thus CyC5 hydrate formation is governed not only by thermodynamic phase considerations but also kinetic factors such as the hydrocarbon/water interfacial area, as well as mass and heat transfer constraints, as for natural gas hydrates. We present a macroscale investigation of the formation and adhesion strength of CyC5 hydrate deposits on bilayer polymer coatings with a range of wettabilities. The polymeric bilayer coatings are developed using initiated chemical vapor deposition (iCVD) of a mechanically robust and densely cross-linked polymeric base layer (polydivinylbenzene or pDVB) that is capped with a covalently attached thin hydrate-phobic fluorine-rich top layer (poly(perfluorodecyl acrylate) or pPFDA). The CyC5 hydrates are formed from CyC5-in-water emulsions, and differential scanning calorimetry (DSC) is used to confirm the thermal dissociation properties of the solid hydrate deposits. We also investigate the adhesion of the CyC5 hydrate deposits on bare and bilayer polymer-coated silicon and steel substrates. Goniometric measurements with drops of CyC5-in-water emulsions on the coated steel substrates exhibit advancing contact angles of 148.3 ± 4.5° and receding contact angles of 142.5 ± 9.8°, indicating the strongly emulsion-repelling nature of the iCVD coatings. The adhesion strength of the CyC5 hydrate deposits is reduced from 220 ± 45 kPa on rough steel substrates to 20 ± 17 kPa on the polymer-coated steel substrates. The measured strength of CyC5 hydrate adhesion is found to correlate very well with the work of adhesion between the emulsion droplets used to form the CyC5 hydrate and the underlying substrates.

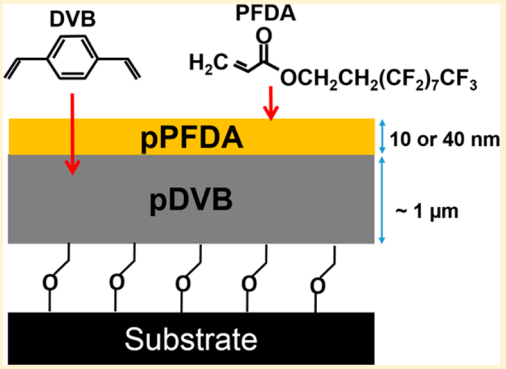


## INTRODUCTION

Clathrate hydrates are crystalline solids resembling ice in which a lattice of space-filling cagelike cavities is made up of hydrogen-bonded water molecules, with the cavities filled by guest molecules stabilizing the lattice structure.[1] The small guest molecules might be hydrocarbons (e.g., methane, ethane, propane), other gases (e.g., carbon dioxide, hydrogen), or liquid (e.g., certain alcohols, tetrahydrofuran, cyclopentane).[2−4] Blockage of oil and gas pipelines via the formation and accumulation of clathrate hydrates is a major concern for the oil and gas industry.[5] Hydrates may also form naturally in oceanic sediments or sediments under the permafrost, where thermodynamic conditions such as high pressures and low temperatures exist.[6,7]

There are active methods to prevent the formation and agglomeration of hydrate inside oil and gas pipelines including external heating of the pipelines,[5,8] addition of water miscible alcohols and glycols such as methanol or ethylene glycol to shift the thermodynamic equilibrium away from typical pipeline conditions,[9] and the use of low-dosage kinetic inhibitors or antiagglomerates to reduce the rate of nucleation and growth of hydrates, or to prevent the agglomeration of hydrate particles into larger structures which increase the risk of blockage.[4,10] Preventing gas hydrate formation inside pipelines using kinetic inhibitors is expensive, has environmental consequences, and is not practical in pipelines with high watercuts. Extensive subcooling in deepwater production impacts effectiveness of kinetic hydrate inhibitors and antiagglomerate (at economically feasible dosages) at watercuts higher than 50−60%.[4,5,8−11] As a consequence, passive methods such as surface modifications of pipeline inner walls are of interest for two reasons: first, in order to minimize nucleation and/or deposition of hydrates on

Received: February 2, 2015
Revised: April 29, 2015
Published: April 30, 2015



  

DOI: 10.1021/acs.langmuir.5b00413
Langmuir 2015, 31, 6186−6196

the pipeline wall, and second, in the case of wall formation or deposition to reduce the hydrate adhesion strength.[12]

We have recently designed and deposited bilayer polymer coatings on steel and silicon substrates through initiated chemical vapor deposition (iCVD). We have shown how these mechanically robust coatings reduce the strength of ice adhesion to underlying silicon and steel substrates more than 6-fold.[13] Using iCVD, it is possible to covalently bond polymeric thin films to the underlying substrates in order to enhance the adhesion of these films and increase their durability against abrasion, erosion, and delamination.[14−16] Another advantage of the iCVD polymer synthesis method is its conformality character which enables deposition of polymers onto rough and nanostructured surfaces without altering the topography of the growth substrate. A thick, densely cross-linked, and hard base layer which is capped with a thin and fluorine-rich top layer resulted in enhanced mechanical properties in the bilayer polymeric films, making them more suitable for application in harsh environments, and thus perhaps in oil and gas pipelines for flow assurance strategies.[13]

At temperatures of industrial interest, hydrates of typical natural gases are only thermodynamically stable at elevated pressures; thus, suitable guest molecules which form hydrates at ambient pressure and moderate temperatures (e.g., above the ice point) are attractive as natural gas hydrate analogues for experimental investigations, due to the advantages in ease of experimental access, visualization, cost, and safety inherent in ambient-pressure experiments. Commonly used ambient-pressure hydrate formers include tetrahydrofuran (THF) and cyclopentane (CyC5). We recently studied the formation and adhesion of THF hydrates on mechanically robust bilayer iCVD polymer films and extended the application of such polymer coatings into the area of durable hydrate-phobic surfaces.[17] This application leveraged the scientific understanding of hydrophobic and icephobic surfaces: specifically, the strong linear correlation between the practical work of adhesion of a single-phase liquid droplet placed on the substrate and the measured adhesion strength of the solid deposit that is subsequently formed from this liquid.

However, because THF is miscible in water, the hydrate formation mechanism may be different than for hydrates of immiscible hydrocarbon/water mixtures, such as those found in oil and gas pipelines. In the present work we investigate the formation and adhesion of CyC5 hydrates to various surfaces. Cyclopentane is a hydrate former which is immiscible with water, and thus CyC5 hydrate formation is governed by the interfacial surface area of the water/guest molecule mixture, and by interfacial transport resistances, as is the case for natural gas hydrates. Studies of the formation mechanism and adhesion of CyC5 hydrates to potential hydrate-phobic surfaces therefore more closely mimic the behavior of natural gas hydrates than does THF hydrate. At ambient conditions, CyC5 hydrate has a dissociation temperature of approximately 7.7 °C and (analogous to the miscible case of THF in water) CyC5 forms a structure II hydrate with water at a molar composition ratio of $H_2O$:CyC5 equal to 17:1.

Formation and adhesion of CyC5 hydrate particles have been investigated in a series of studies by Sloan and co-workers.[1,18−23] Using a micromechanical setup, they examined the adhesion strength between ice and/or hydrate particles.[23−25] Hun et al. also studied the interaction between hydrate particles and water in a temperature-controlled environment utilizing an apparatus fabricated with a microbalance and *z*-axis stage.[26,27] In these studies, capillary force is used to explain the adhesion force between contacting hydrate particles in both wet and dry states. In a recent study, Aspenes et al. investigated the impact of surface energy and the possible presence of other liquids such as water and/or oil in the adhesion strength of hydrates to surfaces. They have shown that the presence of water on solid surfaces results in close to 10 times increase in the adhesion strength of hydrate particles to surfaces.[22]

Several other groups have investigated the bulk formation of CyC5 hydrates from a CyC5-in-water emulsion.[28−30] Morris and co-workers have performed a calorimetric investigation of CyC5 hydrates formed from a water-in-oil emulsion as well as at the interface of water and oil, providing insight into the mechanism of CyC5 hydrate nucleation and growth.[28−30] They have experimentally investigated heterogeneous nucleation of CyC5 hydrates by ice in conjunction with rheological measurements of the properties of hydrate-forming emulsions as the hydrate phase nucleates and grows. Nakajima et al. reported the formation of hydrate from CyC5-in-water emulsions as a potential thermal energy storage media for air-conditioning systems.[31] Sefidroodi et al. investigated the strength and the source of the so-called "memory effect" in the formation of CyC5 hydrates. They observed that if only a few degrees of superheating above the CyC5 hydrate equilibrium dissociation temperature (7.7 °C) are imposed on a sample, then formation of hydrates occurs much more rapidly during subsequent cooling to 0.0 °C, as compared to the case when hydrates are formed from the liquid for the first time.[32]

Despite these extensive studies on the nucleation and growth of CyC5 hydrates, in both particulate and bulk forms, there is a lack of data on their formation and bulk adhesion on engineering substrates of various surface energies. While previously formed hydrate particles may accumulate on pipelines with already formed ice and/or hydrates, in many other applications, hydrate may deposit directly on pipeline walls and form a film.[22] In this situation, and in the absence of external remediation, the deposited hydrate film can grow into a bulk hydrate and the flow path through the pipe becomes obstructed. Brown et al. have used laser-induced fluorescence (LIF) for observing CyC5 hydrate formation and have shown that, in the absence of mixing, hydrate film formation can be observed.[33] There is still a need to study the impact of hydrate crystallization on the adhesion strength of bulk CyC5 hydrates to various engineered surfaces. In the present study, both the bulk formation and subsequent adhesion of CyC5 hydrates to bare and iCVD polymer-coated silicon and steel surfaces are investigated. While a steel substrate is of interest for flow assurance inside commercial oil/gas pipelines, a silicon substrate provides us with a very flat and very rigid reference surface so that we can eliminate the effects of substrate roughness and compliance. A CyC5-in-water emulsion is used to form CyC5 hydrates. Differential scanning calorimetry (DSC) measurements are performed to ensure the presence of hydrates by examining the temperature and latent heat of the CyC5 hydrate dissociation. The strength of CyC5 hydrate adhesion is reduced by a factor of 10 when the bare silicon and steel substrates are coated with the iCVD bilayer polymer coatings. We also measure the advancing and receding contact angles of droplets of a CyC5-in-water emulsion deposited on bare and polymer-coated substrates using goniometry. We find a strong linear correlation between the measured strength of CyC5 hydrate adhesion and the practical work of adhesion



DOI: 10.1021/acs.langmuir.5b00413
*Langmuir* 2015, 31, 6186−6196

between the emulsion droplets and the underlying substrates. The present study of hydrate formation and systematic control of its adhesion to rigid metallic surfaces may be useful in addressing the issue of flow assurance in petroleum pipelines.

We have recently reported the material design and deposition of iCVD bilayer polymeric networks on steel and silicon substrates. Divinylbenzene (DVB) was polymerized and highly cross-linked to form a thick and hard base layer, polydivinylbenzene (pDVB). Subsequently, perfluorodecyl acrylate (PFDA) was polymerized and covalently bonded to the underlying pDVB layer to form a thin and fluorine-rich film, poly(perfluorodecyl acrylate) (pPFDA). This design resulted in bilayer films with enhanced elastic modulus and hardness ($E$ = 19.1 ± 1.2 GPa and $H$ = 479.0 ± 7.0 MPa, respectively), considerable water-repelling nature (advancing water contact angle (WCA) on steel, $\theta_A^w$ = 154.2 ± 2.2°, and receding WCA on steel, $\theta_R^w$ = 150.3 ± 1.6°), and reduced ice and THF hydrate adhesion strength (close to 6-fold and 10-fold reduction in the strength of ice and THF hydrate adhesion, respectively). We also have developed an in situ grafting method to promote the adhesion of the bilayer films to the underlying substrates in order to minimize their delamination and cracking.[13,17]

## EXPERIMENTAL SECTION

**iCVD Coatings.** A custom-built cylindrical reactor was used to perform in situ grafting and iCVD polymerizations (diameter 24.6 cm and height 3.8 cm). An array of 14 parallel chromoalloy filaments (Goodfellow) held around 2 cm from the reactor stage, where the growth substrates are kept, and is used to heat the initiator (*tert*-butyl peroxide, TBPO, 98% Aldrich) during in situ grafting and growth steps.[15,34] A quartz top (2.5 cm thick) covers the reactor allowing real-time thickness monitoring via reflecting a 633 nm He−Ne laser source (JDS Uniphase) off the substrate/polymer and recording the interference signal intensity as a function of time. A mechanical Fomblin pump (Leybold, Trivac) was used to lower the pressure inside the reactor, and an MKS capacitive gauge was used to monitor the pressure. 1*H*,1*H*,2*H*,2*H*-perfluorodecyl acrylate (PFDA, 97%), divinylbenzene (DVB, 80%), and the TBPO (98%) were used as received from Aldrich without any processing. A mass flow controller (1479 MFC, MKS Instruments) was used to adjust and deliver the TBPO at a constant flow rate of 3 sccm during grafting, and 3 and 1 sccm in DVB and PFDA polymerizations, respectively. A dc power supply (Sorensen) was utilized to heat the filament to the desired temperature ($T_f$ = 310 °C during grafting and $T_f$ = 250 °C during pDVB and pPFDA deposition steps). At a filament temperature of $T_f$ = 250 °C only the labile peroxide bond of the TBPO breaks, while at a temperature of $T_f$ = 310 °C methyl radicals can be created as well. Monomers of PFDA and DVB were vaporized inside glass jars through heating of the jars to temperatures of 80 and 60 °C, respectively, and then introduced to the reactor in the vapor phase through needle valves at constant flow rates of 0.1 and 1 sccm, respectively. The temperature of the growth substrate was maintained at $T_s$ = 20 °C during grafting and $T_s$ = 30 °C during polymerization (within ±1 °C) using a recirculating chiller/heater (NESLAB RTE-7). K-type thermocouples (Omega Engineering) were used for measuring all of the temperatures. A throttle valve (MKS Instruments) was used to maintain the desired pressure during grafting and polymerization steps (800 mTorr during grafting and 650 and 300 mTorr in DVB and PFDA polymerizations, respectively). Prior to in situ grafting, growth substrates (silicon wafers from Wafer World Inc. and steel coupons from McMaster-Carr) were first cleaned by sonication in acetone, methanol, and isopropanol each for 5 min, followed by rinsing in deionized (DI) water (>16 MΩ·cm). The substrates were then treated with oxygen plasma for 10 min for further cleaning and enhancing the presence of hydroxyl groups on the substrates before loading to the iCVD reactor.

**DSC Measurements.** A PerkinElmer Pyris 1 DSC was used to determine the temperature and heat of dissociation of ice and hydrate. Temperature and heat calibration were based on the melting point and measurement of the enthalpy of fusion for 99.99% indium. This procedure was further checked using the measured melting temperature and heat of fusion of ice, corresponding more closely with the experimental temperature range. The temperature accuracy is estimated to be ±0.1 °C. Prior to the measurements for the hydrate sample, a small piece of ice (15 mg) was placed inside an aluminum test cell (kept at low temperature inside an ice bucket) and sealed. The test cell was cooled to −20 °C at the rate of −1 °C/min to freeze any free water that might have formed around the ice during handling and placing inside the DSC. This can be confirmed by the appearance of a small exothermic peak in the DSC data during the cooling process (Figure 3c, dashed line). After the test cell was kept at −20 °C for a couple of minutes, the test cell was heated to 15 °C at the rate of 1 °C/min. An endothermic peak at 0.2 °C was observed associated with ice melting. The quantity of heat transferred into the sample by water ice melting, denoted $q_w$, was evaluated by integrating the area under the endothermic peak, and was then divided by the known mass of the water ice (15 mg), which gives $h_w$ = 334.0 kJ/kg for the latent heat of fusion of water ice. Next, a small piece of CyC5 hydrate sample (stored in a temperature-controlled refrigerator at −10 °C and transferred inside an ice bucket for DSC measurements), was placed inside a sample holder similar to the method explained earlier, and underwent through the same process of cooling and heating. The mass of the empty cell was measured and subtracted from the mass of the cell filled with the hydrate (performed after finishing the experiment) to obtain the sample mass, $m$. During the heating, peaks due to the fusion of the ice and dissociation of the hydrate can be observed (Figure 3c, solid line). The quantity of heat transferred into the system to result in fusion of the ice, $q_1$, and dissociation of the cyclopentane hydrate, $q_2$, was calculated from the DSC data. The test cell contains both hydrate and ice, formed during the freezing of the free water. The mass of water, $m_w$, was obtained from the following relation:

$$m_w = q_1/h_w \quad (1)$$

The mass of cyclopentane hydrate in the cell was obtained by subtracting the mass of free water, $m_w$, from the total mass, $m$:

$$m_h = m - m_w \quad (2)$$

The latent heat of the hydrate dissociation, $h_h$, was then calculated using the following relation:

$$h_h = q_2/m_h \quad (3)$$

**Surface Tension and Contact Angle Measurements for CyC5-in-Water Emulsion.** A goniometer equipped with an automated dispenser (Model 500, ramé-hart) was used to measure the surface tension of the CyC5-in-water emulsion and the advancing and receding contact angles of the emulsion droplets on the bare and polymer-coated silicon and steel substrates. A pendant drop method was used to obtain the effective surface tension of the stable CyC5/water emulsion.[35] Measurements were performed on the as-made emulsion and 4 h after preparation. In both cases, the measurement was done rapidly after sampling the emulsion from sealed glass vials to minimize the impact of air exposure on the cyclopentane droplets in the emulsion. The surface tension values were ensemble averaged from measurements on 10 separate droplets. The sessile drop method is used to obtain the advancing and receding contact angles of the emulsion on substrates using a 5 μL CyC5 emulsion droplet placed on the surface of interest and then incrementally increasing/decreasing the droplet volume by approximately 0.15 μL until advancing and receding in the contact angle of the emulsion droplet are observed.[36] Each reported contact angle value is the average of values obtained from the goniometer measurements using five emulsion macro-droplets.

**Strength of CyC5 Hydrate Adhesion Measurements.** A custom-built apparatus was used to examine the adhesion strength of the CyC5 hydrates on bare and polymer-coated substrates.[21,37] The





DOI: 10.1021/acs.langmuir.5b00413
*Langmuir* 2015, 31, 6186−6196

substrates were cut into 1.5 cm × 1.5 cm pieces and clamped to a base plate. Glass cuvettes (1 cm × 1 cm cross section and 4 cm tall) were approximately 90% filled with the CyC5-in-water emulsion and placed inside a holder. The base plate which contains clamped substrates was placed on top of the cuvette holder. The cuvette holder and the base plate were fastened with screws and gently inverted to allow direct contact of the CyC5 emulsion inside the cuvettes with the substrates (both bare and polymer-coated silicon and steel). Any residual emulsion on the substrates and outside of the cuvettes was removed to prevent the formation of any solid outside of the cuvettes. To form hydrates, the samples underwent the same thermal conditioning explained earlier using a Peltier plate (TECA Corp., Model LHP-800CP) in a humidity-controlled glovebox (humidity <5%). After hydrate formation, the probe of a force transducer (Imada, Model ZP-44), mounted on a single axis translation stage, was used to apply a progressively increasing shear force to the cuvettes, and the maximum force required to break the crystal solid−substrate interface was recorded. The distance of the probe and the substrates was about 1.3 mm to minimize applying torque to the hydrate−substrate interface, and maintained the same during all of the measurements. For each type of sample, 20 adhesion tests were performed to reduce statistical variations in the reported data. The measured CyC5 hydrate adhesion force divided over the cross section of the glass cuvettes (1 $cm^2$) to obtain the shear strength of CyC5 adhesion.

## RESULTS AND DISCUSSION

Our previous work extensively describes the design and polymerization of bilayer films via the iCVD method.[13] Thus, we only provide a brief summary in this section.

First, we clean chosen growth substrates (e.g., silicon wafers or steel coupons) with solvents (e.g., acetone, methanol, and isopropanol) and then through exposure to oxygen plasma to further enhance the presence of hydroxyl groups on the surfaces. Next, we load the treated substrates into the iCVD reactor to perform grafting and subsequent deposition of pDVB and pPFDA layers without breaking the vacuum. For grafting, we keep the growth substrate at $T_s$ = 20 °C and introduce *tert*-butyl peroxide (TBPO) in a vapor form to create methyl radicals via filament heating ($T_f$ = 310 °C).[38,39] These radicals can react with the hydroxyl groups of the plasma-treated growth substrates and create activated surface sites to form covalent bonds between the substrate and the bilayer film. To deposit the base layer (pDVB), we introduce DVB, $N_2$, and TBPO simultaneously with the flow rates of 1, 1, and 3 sccm, respectively, while maintaining the filament and substrate temperatures of $T_f$ = 250 °C and $T_s$ = 30 °C, respectively.[40] A densely cross-linked layer of pDVB can be deposited through this step in the desired thickness (in the range 200 nm−1 μm). We measure the thickness of both polymeric layers using ellipsometry (details are given in our previous study).[13]

Finally, we grow our fluorine-rich top layer (pPFDA) through introducing PFDA, $N_2$, and TBPO at the flow rates of 0.1, 1, and 1 sccm, respectively, while maintaining the same filament and substrate temperatures ($T_f$ = 250 °C and $T_s$ = 30 °C). Through this final step, pPFDA in two thicknesses is deposited (10 or 40 nm thick) on both flat silicon (henceforth denoted as "BL (10 nm) on Si" and "BL (40 nm) on Si" respectively) and rough steel substrates (henceforth denoted as "BL (10 nm) on steel" and "BL (40 nm) on steel"). While a thick pPFDA film (40 nm) can ensure a more complete coverage of the bilayer film, the presence of the densely cross-linked pDVB network underneath a very thin 10 nm pPFDA film can prevent inward reorientation of fluorine groups in the pPFDA top layer when it is exposed to water, resulting in lower water contact angle hysteresis ($\theta_A^w - \theta_R^w$).[41] A summary of water contact angle (WCA) measurements on BL (10 nm) and BL (40 nm) coatings deposited on flat silicon and rough steel substrates is presented in Table 1.

**Table 1. Contact Angles for Droplets of Water and CyC5-in-Water Emulsion Obtained from Goniometric Measurements on Bare Si and Steel, and on Linker-Free Grafted Bilayers of pDVB/pPFDA[a]**

| | water contact angle | | emulsion contact angle | |
|---|---|---|---|---|
| | receding $\theta_R^w$ (deg) | advancing $\theta_A^w$ (deg) | receding $\theta_R$ (deg) | advancing $\theta_A$ (deg) |
| bare Si | 9.6 ± 1.5 | 32.2 ± 2.8 | 9.1 ± 1.7 | 32.5 ± 2.1 |
| BL (40 nm) on Si | 132.0 ± 7.8 | 149.1 ± 1.9 | 122.1 ± 7.5 | 135.7 ± 6.7 |
| BL (10 nm) on Si | 145.0 ± 1.8 | 152.0 ± 1.0 | 140.5 ± 6.6 | 147.6 ± 5.4 |
| bare steel | 19.9 ± 3.7 | 76.0 ± 6.5 | 17.2 ± 3.5 | 63.1 ± 6.0 |
| BL (40 nm) on steel | 143.2 ± 1.7 | 152.0 ± 2.1 | 125.2 ± 10.1 | 138.5 ± 7.5 |
| BL (10 nm) on steel | 150.3 ± 1.6 | 154.2 ± 2.2 | 142.5 ± 9.8 | 148.3 ± 4.5 |

[a]Two bilayer coatings are studied; both consist of a densely cross-linked pDVB network and then either (i) a thicker top layer of approximately 40 nm pPFDA deposited on underlying substrates of silicon and steel (denoted "BL (40 nm) on Si" and "BL (40 nm) on steel", respectively), or (ii) a thinner top layer of approximately 10 nm pPFDA on Si and steel (denoted "BL (10 nm) on Si" and "BL (10 nm) on steel"). These data indicate the emulsion-repelling nature of the bilayer polymeric coatings.

Fourier transform infrared (FTIR) spectroscopy and X-ray photoelectron spectroscopy were performed on the bilayer polymer networks and confirmed successful deposition of both pPFDA and pDVB components through the presence of bands corresponding to carbonyl, carbon−fluorine bonds, and phenyl groups in the FTIR spectra.[13] The properties of the BL films can be summarized as follows. Optical profilometer measurement gave root-mean-square (RMS) roughness values of $R_q$ = 34.2 ± 5.2 nm and $R_q$ =28.3 ± 3.8 nm for BL (40 nm) on Si and BL (10 nm) on Si, respectively.[13] In addition, RMS roughness values of $R_q$ = 132.5 ± 17.4 nm and $R_q$ = 120.3 ± 22.0 nm were obtained from measurements performed on BL (10 nm) on steel and BL (40 nm) on steel samples, respectively. The increase in the RMS roughness value of the bilayer polymer film when deposited on the steel coupons (as compared to the value measured on the silicon wafer) comes from the roughness of the underlying steel substrate. The elastic moduli and hardnesses of the bilayer films were obtained from nanoindentation measurements, giving values (on silicon substrates) of $E$ = 19.1 ± 1.2 GPa and $H$ = 479.0 ± 7.0 MPa for the 40 nm bilayer films and $E$ = 18.1 ± 1.0 GPa and $H$ = 463.0 ± 4.5 MPa for the thinner 10 nm films. It is important to note that the elastic modulus and hardness are controlled primarily by the densely cross-linked pDVB network and not by the thin top layer pPFDA film or the underlying substrate; therefore, both the BL (40 nm) and the BL (10 nm) films showed comparable elastic modulus and hardness values on silicon and steel substrates.[13]

**Formation of CyC5-in-Water Emulsion.** Emulsions of CyC5 (Sigma-Aldrich, ≥99%) and deionized water, in which





DOI: 10.1021/acs.langmuir.5b00413
*Langmuir* 2015, 31, 6186−6196

4% Tween 85 (Sigma-Aldrich) was first dissolved to serve as an emulsifier, were prepared in sealed glass vials by 30 min of ultrasonication (Aquasonic 150D, VWR at a power level of 9).[42] The water-to-CyC5 molar ratio in every sample was held fixed at approximately 17:1, in agreement with the stoichiometric host-to-guest molar ratio in a structure II hydrate with full occupation of its $5^{12}6^4$ cages by guest molecules.[31] A freshly prepared emulsion sample was transferred into a rectangular capillary placed on a glass slide for imaging under the microscope. Figure 1 shows representative photomicrographs

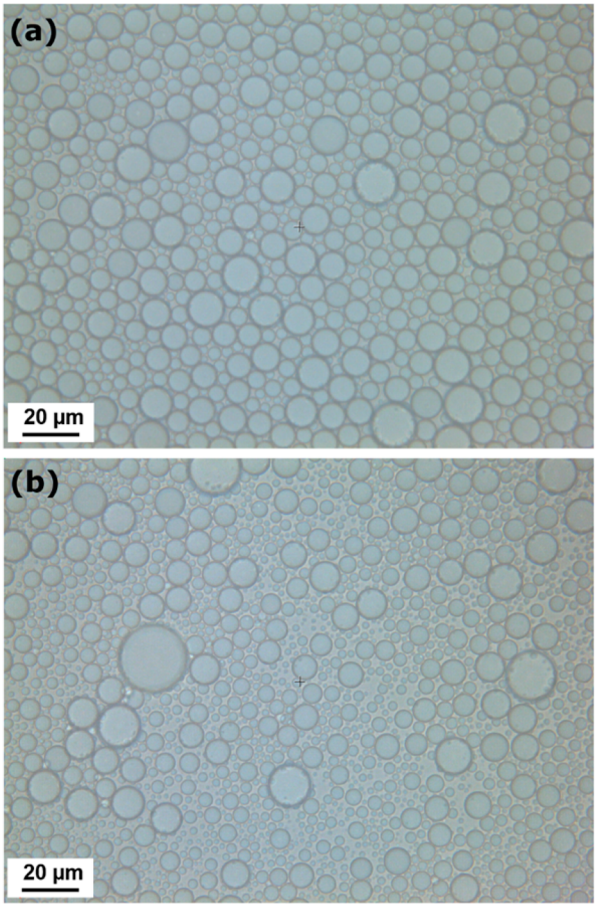


**Figure 1.** Representative emulsion photomicrographs taken of as-made emulsion (top) and 4 h after preparation (bottom). Using 10 photomicrographs at each time, the mean droplet diameter was observed to decrease from an ensemble-averaged value of 8.4 ± 3.8 $\mu$m to 5.8 ± 3.4 $\mu$m after 4 h. Thus, the emulsions are sufficiently stable to perform hydrate formation experiments by extended cooling.

of the as-made emulsion and again 4 h after preparation. The glass vials were gently inverted a few times before sampling for these images. The Tween 85 surfactant helps stabilize the emulsion against rapid coalescence, and the droplet size distribution only changes slowly over a period of 4 h (see Table 2). The droplet diameter, averaged over 10 independent

**Table 2. Droplet Size Distribution of Hydrate-Forming CyC5-in-Water Emulsion as a Function of Time**

| time (h) | mean drop size ($\mu$m) | std dev ($\mu$m) |
|---|---|---|
| 0 | 8.4 | 3.8 |
| 4 | 5.8 | 3.4 |

samples, changed from 8.4 ± 3.8 $\mu$m to 5.8 ± 3.4 $\mu$m after 4 h, which provides sufficient stability of the emulsions to perform hydrate formation experiments by extended cooling. The large standard deviations measured arise from both sample-to-sample variations and a slow change in the droplet size. The emulsion was also found to be relatively stable against rapid coalescence when maintained at −15 °C as well.

**Formation of CyC5 Hydrates.** To study the formation of CyC5 hydrates, approximately 4 mL of the stabilized CyC5-in-water emulsion was poured into a glass cuvette and placed on a Peltier cold plate inside a custom-built transparent acrylic box. A steady nitrogen flow was maintained inside the acrylic box to ensure low humidity and to prevent frost formation. The temperature of the cold plate decreased to −15 °C within several minutes and was maintained for 30 min to ensure the formation of ice/hydrate. Visual observation of the formation of CyC5 hydrates was performed by a digital camera with a macro lens (EOS 7D).

Figure 2 shows snapshots obtained by viewing the sample through the transparent acrylic box and glass cuvette (see Supporting Information for a video of hydrate formation). Figure 2a shows the stabilized emulsion of CyC5 droplets in water before cooling to low temperature. Figure 2b–d shows the nucleation and growth of the ice/hydrate phase while the substrate temperature was held at −15 °C. As time passes and thermal energy is removed from the system by the Peltier plate, the sample in the cuvette mostly turns into a solid. The temperature of the cold plate was then increased incrementally (0.5 °C/min) until it reached 0.0 °C (Figure 2e) and was maintained at this temperature for 5 min to allow melting of any ice that may be formed. Figure 2f shows that, upon warming to 0.0 °C, ice was observed to melt from the periphery of the cuvette leaving a core hydrate. To ensure the entire sample experiences a temperature above the equilibrium ice melting point (and to melt any residual ice), the temperature was then increased to 2 °C (Figure 2g). Hydrate formation occurs simultaneously with ice melting as soon as there is free water at the oil/water interface of the frozen CyC5 slurry. CyC5 hydrate formation could be visually observed to start when the CyC5-in-water emulsion became cloudy and dark. The dark and cloudy appearance in the solid inside the cuvette is indicative of formation of the hydrate. Finally, the temperature was increased gradually (in approximately 0.3 °C/min increments) until it reached 5 °C (Figure 2h) to allow further ice melting which provides free water at the interface with CyC5. The temperature was then maintained at this temperature for 60 min (Figure 2i) to ensure melting of ice and the equilibration of the microstructure. Any remaining solid in the cuvette at 5 °C must be a CyC5 hydrate ($T_M$ = 7.7 °C). The ice, which melts away during warming, provides free water and thus the core slushy remnants act as sites for reforming hydrates while stabilizing the temperature (e.g., at 5 °C) just below the equilibrium hydrate forming point.

The cyclopentane hydrate formation process is an interfacially mediated phenomenon that proceeds with a rate that depends on the availability of interfacial area between the water and the hydrate former (CyC5). Using the protocol described above, CyC5 hydrates can be prepared without continuous agitation of the emulsion. The rapid initial cooling of the emulsion results in locking-in of the emulsion droplets before coalescence. When the temperature is raised just above the ice melting point, the high contact area between the continuous phase liquid water and the dispersed oil drops


DOI: 10.1021/acs.langmuir.5b00413
Langmuir 2015, 31, 6186–6196

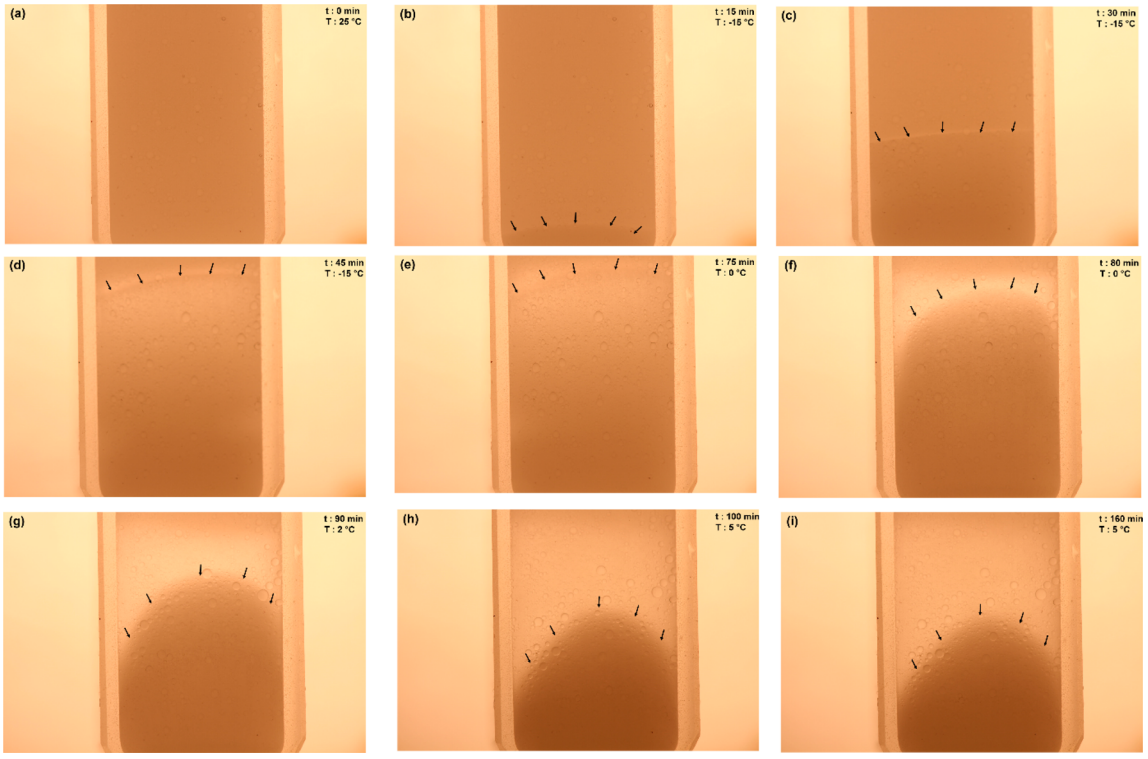


**Figure 2.** Pictures of cyclopentane hydrate formation from a 17:1 (mole ratio) water:cyclopentane emulsion inside a glass cuvette, taken during visual observation by camera. Arrows indicate the interface of the solid and the emulsion. A video of hydrate formation can be accessed in the Supporting Information. The cross section of the cuvette is 1 cm × 1 cm.

promotes nucleation and growth of the cyclopentane hydrate. Zhang et al.[42] and Karanjkar et al.[28] also observed the formation of hydrate without continuous agitation in their DSC studies of hydrate formation. In addition, Aman et al. used cyclical DSC measurements to study the stabilizing effects of surfactants present in hydrate dispersions formed from water-in-oil emulsions.[19] In our work, the interfacial area between the water and the CyC5 is higher than previous literature reports due to the small size of the CyC5 droplets (~5−10 $\mu$m in diameter).[28] Considering the microscopic size of the CyC5 droplets, it was not possible to image through the bulk hydrate due to light scattering effects. For this reason, we rely on direct visual observation of hydrate formation to show the interface between the hydrate phase and the emulsion. Blank negative control tests with no CyC5 were carried out intermittently to check that no ice/hydrate formed from samples containing only water that underwent the identical thermal cycling procedure.

**Differential Scanning Calorimetry Measurements.** After the hydrate formation process was finished, a small quantity of the formed hydrate was sampled from the cuvette and then subjected, after overnight storage in a refrigerator at approximately −10 °C, to a measurement of the heat of hydrate dissociation by differential scanning calorimetry (DSC). Parts a and b of Figure 3 show pictures taken from the CyC5 hydrate inside a cuvette and a small piece sampled for the DSC measurements, respectively. The test cell used for the DSC measurements was made of aluminum and sealed with an aluminum cap. A PerkinElmer Pyris 1 DSC calibrated with 99.99% standard indium was used for calorimetric studies. The working principle is based on differential measurement of the temperature of a sample and the reference; the necessary heat flow required to achieve a zero difference between the two is recorded as an output.[28] Prior to the measurement of the

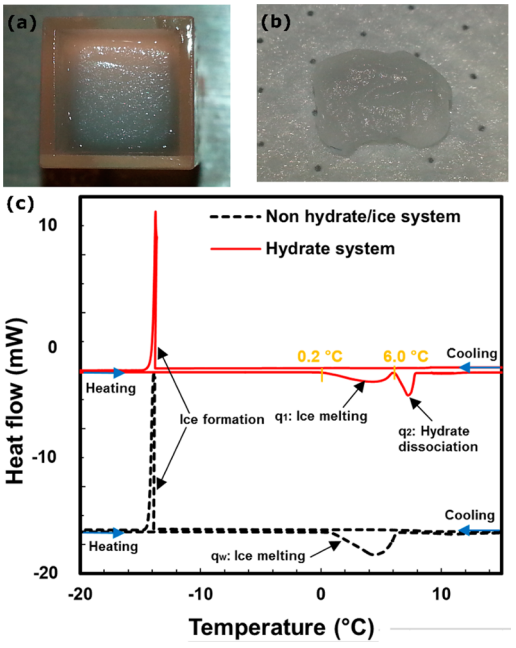


**Figure 3.** Photographs of (a) the CyC5 hydrate formed inside a cuvette, and (b) a small piece of CyC5 hydrate sampled from the cuvette for the DSC measurements. (c) DSC thermograph of hydrate system (red solid line) and non-hydrate-containing (pure water/ice) system (black dashed line). The heating and cooling rates were 1 °C/min. Data for the non-hydrate/ice system is shifted downward for the clarity. The hydrate system shows two separate peaks during heating corresponding to ice melting and hydrate dissociation whereas the non-hydrate/ice system only shows a single ice melting peak.





DOI: 10.1021/acs.langmuir.5b00413
*Langmuir* 2015, 31, 6186−6196

hydrate samples, the latent heat and the temperature of fusion of a non-hydrate-containing (100% water−ice) system was measured for use as a comparative standard for evaluating the latent heat and the dissociation temperature of an ice/hydrate system from the relevant DSC data. The Experimental Section details the test procedure.

Figure 3c compares the heat flow curves in a DSC trace of the hydrate and the non-hydrate/pure ice systems for the same temperature protocol. Since, inevitably, some fraction of the sample in both the hydrate-containing and non-hydrate systems was melted during the procedure of sample loading into the test cell, each sample was first subcooled in order to freeze any residual free water. The temperature was decreased from 15 to −20 °C and then brought back to 15 °C at a fixed ramp rate of 1 °C/min in each direction. DSC data shows an exothermic peak during the cooling ramp in both systems, due to freezing of free water and the formation of an ice shell. Karanjkar et al. have observed a single exothermic peak during cooling based on an energy balance and concluded that there is only ice formation in this step.[28] Fouconnier et al. observed a similar single exothermic peak during cooling, and they utilized X-ray diffraction coupled with DSC to separate ice formation, ice melting, hydrate formation, and hydrate dissociation peaks.[43] The ice formation exothermic peak is around −15 °C for both systems. This is close to the ice formation peak reported by Karanjkar et al.[28] (∼ −20 °C) but significantly higher than the ice nucleation temperature of −38 °C reported by Clausse.[44] In addition, an asymmetry was observed in the ice formation peak which is in contrast to Clausse.[44] Karanjkar et al.[28] have argued that the disagreement with Clausse's measurements might be due to some crowding of droplets due to gravitational settling of water drops.[28,44] In addition, a stable water-in-oil emulsion at water contents up to around 30 vol % exhibits an ice freezing peak at around −38 °C which in nature is different than our emulsions of cyclopentane-in-water (1:17 molar ratio). Zhang et al. also observed an exothermic peak around −15 °C which is believed to be related to the heterogeneous nucleation of ice.[42] Once ice nucleation occurs, they speculated that the water drops may undergo a rapid phase change with energy release characteristics similar to that observed for bulk water.

Upon subsequent heating there is an endothermic peak observed in both systems near 0.2 °C relevant to energy uptake as a result of ice melting. In the hydrate system, during heating an additional endothermic peak corresponding to the hydrate dissociation was observed in the range of 6−7 °C. This is close to the phase-equilibrium temperature ($T_{eq}$) of CyC5 hydrate that has been previously reported in the literature (6.6 °C ≤ $T_{eq}$ ≤ 7.7 °C).[28,31]

The area under the endothermic peaks measured during heating provides the latent heat associated with ice melting and hydrate dissociation. From the non-hydrate system, the latent heat of fusion of water ice was found to be $h_w$ = 334 kJ/kg, which is very close to the reference value of the heat of fusion for ice at atmospheric pressure, $h_w$ = 333.427 kJ/kg.[45] This can be used as the standard for the evaluation of the heat of hydrate dissociation from the DSC data. For the hydrate system, the latent heat of CyC5 hydrate dissociation was measured to be 117.4 kJ/kg (see the Experimental Section for details). Nakajima et al. have reported that the effective heat of dissociation of CyC5 hydrate masses with no dewatering procedure ranges from 41 to 220 kJ/kg.[31] They have also shown a tendency for an asymptotic increase in the heat of hydrate dissociation with an increase in the surfactant concentration.[31] In addition, a dewatering procedure has shown promise in effectively increasing the heat of hydrate dissociation.[31,42]

**Wettability of Bilayer iCVD Polymer-Coated Surfaces by Emulsion Droplets.** The CyC5-in-water emulsion was prepared in a manner similar to the protocol explained in the previous section, and its effective interfacial tension and impact on wettability of surfaces (iCVD bilayer polymer-coated and bare substrates) were studied. The effective interfacial tension of the CyC5-in-water emulsion was measured through the pendant drop method.[35] Measurements were performed on the as-made emulsion and again 4 h after its preparation. Following the same procedure as used for obtaining the microphotograph images, the glass vials containing the emulsion were inverted gently a few times prior to sampling for the goniometry measurements. The effective surface tension for the emulsion in air was found to be 59.3 ± 1.8 mN/m, averaged from measurements of 10 droplets of as-made emulsion and samples taken 4 h after emulsification. The surface tensions of distilled water (71.0 ± 1.0 mN/m) in air and CyC5 (24.2 ± 0.8 mN/m) in air were also measured independently and used for confirming the accuracy of the tensiometry measurements. Given the high molar ratio of water/CyC5 (17:1) and the fact that the emulsion consists of discrete cyclopentane droplets in a continuous water phase with a small amount of additional surfactant, it is to be expected that the effective interfacial tension of the emulsion is signifcantly higher than the surface tension of pure CyC5 and is closer to the surface tension of water.[5]

The wettability of the bare substrates and the iCVD polymer bilayer coatings by the emulsion was also investigated. Contact angle measurements provide a useful tool for probing interfacial interactions between a solid and a liquid. The wettability of a surface by a pure liquid or a mixture can be enhanced by either reducing the liquid surface tension or by increasing the substrate surface energy. In Table 1 and Figure 4 we show the measured advancing and receding contact angles of CyC5-in-water emulsion droplets on bare and coated silicon and steel substrates. In Figure 4b we show representative emulsion droplet images captured during the contact angle measurements on bare Si (top), BL (40 nm) on Si (middle), and BL (10 nm) on Si (bottom). The cyclopentane microdroplet diameter in the macroscopic liquid drop of emulsion, averaged over 10 independent samples, was 8.4 ± 3.8 μm. The bare Si substrate is hydrophilic and exhibits both low advancing (32.5 ± 2.1°) and receding (9.1 ± 1.7°) contact angle values for the emulsion drop. The linker-free grafted bilayer pDVB/pPFDA polymer with a top pPFDA thickness of ∼40 nm on Si (BL (40 nm) on Si) resulted in much higher advancing ($\theta_A$ = 135.7 ± 6.7°) and receding ($\theta_R$ = 122.1 ± 7.5°) contact angles for the emulsion droplets due to the high density of fluorine-containing groups in the pPFDA layer. Corresponding values for water contact angles (WCAs) on this substrate are even higher ($\theta_A^w$ = 149.1 ± 1.9° and $\theta_R^w$ = 132.0 ± 7.8°), which is consistent with the higher surface tension of a water droplet when compared to CyC5-in-water emulsion.[13] Small variations in the measured contact angles might be due to local differences in the surface morphology or crystallinity of the top pPFDA layer which can arise from variations in the polymer deposition.[15,34] The 40 nm pDVB/pPFDA bilayer was also deposited on the steel surface and resulted in advancing and receding contact angles for the emulsion droplets of $\theta_A$ = 138.5 ± 7.5° and $\theta_R$ = 125.2 ± 10.1°, respectively. The increase in the



DOI: 10.1021/acs.langmuir.5b00413
Langmuir 2015, 31, 6186−6196

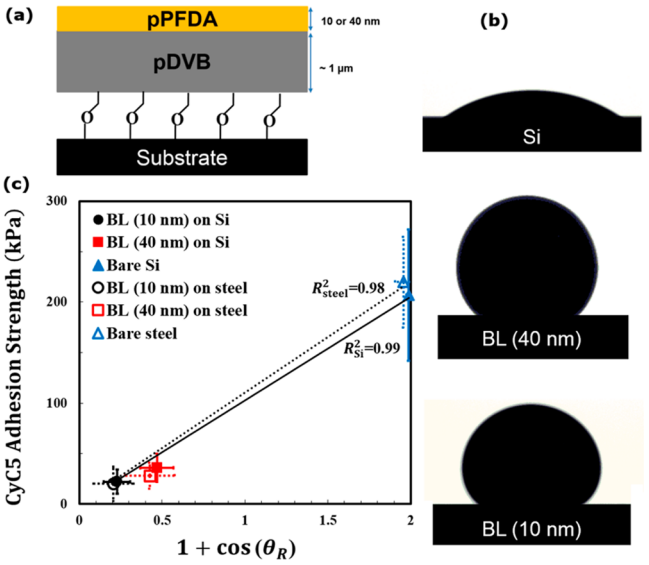


**Figure 4.** (a) Schematic of the bilayer polymer network deposited on a substrate. (b) Representative images of CyC5-in-water emulsion droplets captured during contact angle measurements on bare Si (top), linker-free grafted bilayer pDVB/pPFDA with 40 nm pPFDA on Si (denoted "BL (40 nm) on Si") (middle), and linker-free grafted bilayer pDVB/pPFDA with 10 nm pPFDA on Si ("BL (10 nm) on Si") (bottom). (c) Adhesion strength of CyC5 hydrates as a function of the scaled work of adhesion of the CyC5-in-water emulsion on bare and polymer coated substrates. $W^{adh} = \gamma_{LV}(1 + \cos\theta_R)$, where $\gamma_{LV}$ = 59.3 ± 1.8 mN/m. The data suggest that the adhesion strength of the cyclopentane hydrate to the surface correlates well with the work of adhesion of the liquid emulsion used to form the CyC5 hydrates ($R^2_{steel}$ = 0.98 and $R^2_{Si}$ = 0.99). These data suggest that relatively simple goniometric measurements of CyC5-in-water emulsion droplets can be used as a probe fluid to obtain the work of adhesion and predict the strength of CyC5 hydrate adhesion on a given substrate, which is an extremely challenging experimental measurement. The cyclopentane microdroplet diameter in the macroscopic emulsion droplet, averaged over 10 independent samples, was 8.4 ± 3.8 μm.

measured advancing and receding contact angles for the emulsion droplets over the values measured on the silicon substrate is due to the enhanced surface roughness of the linker-grafted polymer film that originates from the underlying rough steel substrate.[46]

The linker-free grafted bilayer film (pDVB/pPFDA) with a thinner pPFDA top layer (~10 nm) was also deposited on the silicon substrate (denoted "BL (10 nm) on Si"), and this resulted in an increase in both the advancing ($\theta_A$ = 147.6 ± 5.4°) and receding ($\theta_R$ = 140.5 ± 6.6°) contact angles for the CyC5 emulsion droplets. We have observed similar trends in the advancing and receding contact angles for water droplets on 10 nm thick pPFDA layer as well ($\theta^w_A$ = 152.0 ± 1.0° and $\theta^w_R$ = 145.0 ± 1.8°).[13] Similar to the trends reported above for the thicker pPFDA layer (40 nm), a slight increase in the contact angles for the emulsion droplets on the thin bilayer film deposited on steel substrates (denoted "BL (10 nm) on steel") was observed ($\theta_A$ = 148.3 ± 4.5° and $\theta_R$ = 142.5 ± 9.8°), when compared to the polymer films deposited on Si substrates.

In summary, a decrease in the contact angle hysteresis ($\theta_A - \theta_R$) for droplets of water and for the CyC5 emulsion is observed when the pPFDA layer thickness is decreased to ~10 nm on both substrates (Si and steel). We have shown in our previous studies that the presence of the densely cross-linked and rigid pDVB network underneath an ultrathin pPFDA film (~10 nm) can prevent inward reorientation of the fluorine groups in the pPFDA layer when exposed to partially wetting liquids and this results in the lower contact angle hysteresis that is observed macroscopically (see Supporting Information, Figure S1).[41] It is to be noted that all of the substrates are wetted by pure CyC5 droplets due to the very low surface tension of cyclopentane. Overall, the thinner bilayer coating (10 nm) shows enhanced repellency to an emulsion of CyC5-in-water when compared to a thicker bilayer (40 nm) on both substrates, and this suggests that the latter coating is likely to perform better at reducing the strength of CyC5 hydrate adhesion.

**CyC5 Hydrate Formation and Strength of Its Adhesion to Surfaces.** Next, we study the formation of CyC5 hydrates and the strength of their adhesion to bare surfaces and polymer-coated substrates with two different top layer thicknesses (BL (10 nm) and BL (40 nm)). A custom-built adhesion testing apparatus housed inside a nitrogen-containing glovebox was used for this purpose (Supporting Information, Figure S2).[13] The CyC5-in-water emulsion was prepared similarly to the method explained earlier, poured into glass cuvettes, and then underwent the same thermal conditioning process described earlier to ensure formation of CyC5 hydrates on the substrates inside the cuvettes.[12] Care was taken to minimize air exposure of the emulsion, and the time elapsed between its preparation and pouring into cuvettes for the strength of adhesion measurements was also kept to a minimum (less than a minute) in order to minimize CyC5 evaporation and emulsion droplet coalescence.

The lateral force required to fracture the frozen cuvettes from the substrate was recorded and converted into a measure of the shear strength of CyC5 hydrate slurry adhesion by dividing over the cuvette area. The measurements were performed on 20 samples of each type and then ensemble averaged. Sample-to-sample variations in the measured adhesion strengths are largely due to the dominant role of local flaws in adhesive failure tests and local variations in the nature of the CyC5 hydrate formed at the interface with the substrate. Another factor contributing to variations in the data might be possible differences in hydrate numbers as some cages in the hydrate structures formed might not be occupied with CyC5 guest molecules.[47]

The strength of CyC5 hydrate adhesion on bare silicon substrates was measured to be 207 ± 65 kPa, whereas on the bilayer polymer coatings, BL (40 nm) on Si and BL (10 nm) on Si, it was reduced to 36 ± 14 kPa and 22 ± 12 kPa, respectively. Steel substrates coated with a linker-free bilayer of the perfluorinated pPFDA polymer (BL (10 nm) on steel) resulted in CyC5 hydrate adhesion strength of 20 ± 17 kPa, which is a 10-fold reduction when compared to the corresponding adhesion values measured on bare steel substrate (220 ± 45 kPa). There is an enhanced reduction in the strength of CyC5 hydrate adhesion on the thinner BL (10 nm) when compared to the thicker BL (40 nm) on both substrates (Si and steel) which is consistent with the enhanced liquid repellency to CyC5-in-water emulsion droplets observed on both substrates for the thinner pPFDA film.

It may be conjectured that there is a difference between the actual temperature inside the cuvettes and the cold plate temperature. Therefore, to understand possible differences in the nature of the formed CyC5 hydrates and the strength of their adhesion to the different substrates, adhesion measure-





DOI: 10.1021/acs.langmuir.5b00413
Langmuir 2015, 31, 6186−6196

ments were also carried out at cold plate temperatures of +2 and +4 °C. While Corak et al. have shown that the kinetics of hydrate formation at lower levels of subcooling are significantly slower than the kinetics at higher subcooling temperatures,[47] we find that the measured adhesion strength values are within the same range, indicating minimal impact, if any, of the subcooling temperature in this temperature range. This finding is in accord with Zhang's observation.[42]

**Relation between Surface Wettability and the Strength of CyC5 Hydrate Adhesion.** It has been shown that the wettability and motion of liquid droplets on surfaces involve two distinct kinematic processes: shear and tensile.[48−50] While shear deformation is related to sliding and/or roll-off of liquid droplets from surfaces (shear hydrophobicity), tensile deformations are more closely related to measurements of the pull-off force required to detach a droplet from a surface (tensile hydrophobicity). This latter quantity is related to the specific work of adhesion between a liquid droplet (e.g., a droplet of CyC5-in-water emulsion) and the underlying substrate and can be calculated from the Young−Dupré equation:[48−50]

$$W^{adh} = \gamma_{LV}(1 + \cos\theta_R) \quad (4)$$

where $W^{adh}$ is the work of adhesion between a liquid droplet (e.g., a drop of CyC5-in-water emulsion) and the underlying substrate, $\gamma_{LV}$ is the surface tension between the liquid (e.g., a drop of CyC5-in-water emulsion) and air, and $\theta_R$ is the receding contact angle of the CyC5-in-water emulsion droplet on a substrate.

A high receding contact angle of a CyC5-in-water droplet on a substrate corresponds to low pull-off forces under tensile (normal) loading conditions. To reflect the importance of tensile hydrophobicity, we present our results for the strength of CyC5 hydrate adhesion by plotting the measured values obtained from the adhesion apparatus versus the work of adhesion between a liquid droplet (i.e., the CyC5-in-water emulsion) and a given substrate (either bare or polymer coated). Figure 4c shows that the average strength of CyC5 hydrate adhesion linearly reduces with decreases in the work of adhesion of an emulsion droplet placed on either substrate (with correlation coefficients $R^2_{steel} = 0.98$ and $R^2_{Si} = 0.99$). The trend observed in this data is consistent with our previously observed trend in the strength of ice adhesion on icephobic coatings[13] and suggests that the adhesion strength of CyC5 hydrate on an underlying substrate correlates well with the work of adhesion of a CyC5-in-water emulsion droplet, from which the hydrate phase will subsequently nucleate and grow on the cooled substrate.

Overall, very good linear correlation between the measured hydrophobicity of CyC5-in-water emulsion droplets placed on the deposited polymer films and their corresponding hydrate-phobic behavior is observed. These results confirm that surfaces with stronger CyC5-in-water emulsion repelling character are optimal for reducing the strength of CyC5 hydrate adhesion. The reduction in the strength of hydrate adhesion reported in this work is higher than those values reported elsewhere for soft fluorinated polymer coatings.[37,51] The high modulus and stiffness of the cross-linked polymer networks that are deposited by the iCVD process prevent surface remodeling when wetted and also provide greatly enhanced mechanical resistance to the wear and erosion processes that are characteristic of industrial applications. Future studies should investigate the repelling character of different substrates toward emulsion droplets on the microscale (corresponding to the length scale of individual droplets) and its relation to macroscopic goniometric measurements of emulsion droplets, as well as the subsequent impact on the strength of macroscale cyclopentane hydrate adhesion to different rough textured substrates.

## CONCLUSION

In conclusion, we have studied the formation and deposition of cyclopentane (CyC5) hydrates from subcooled CyC5-in-water emulsions and the adhesion of these hydrates to thin cross-linked fluorinated bilayer polymer coatings. The large CyC5/water interfacial area in the emulsions yield high rates of hydrate formation when the emulsion is cooled below the hydrate phase equilibrium temperature. Visual imaging allowed direct observation of hydrate formation, and DSC measurements verified formation of the CyC5 hydrate and calculation of the heat of CyC5 hydrate dissociation. Contact angle measurements of emulsion droplets placed on the iCVD-coated surfaces revealed the emulsion-repelling nature of the mechanically robust bilayer polymer films we have developed. The bilayer pDVB/pPFDA polymer coatings reduced the strength of CyC5 hydrate adhesion by up to 10-fold. We found a strong linear correlation between the measured strength of CyC5 hydrate adhesion and the practical work of adhesion calculated via the Young−Dupré equation for a droplet of CyC5-in-water emulsion that is placed on the underlying substrate. The results of this work suggest that the CyC5-in-water emulsion can be effectively used as a probe liquid for evaluating the adhesion strength of CyC5 hydrates on different coatings. The 10-fold reduction in hydrate adhesion on the cross-linked pDVB network capped with a very thin pPFDA coating offers a pathway forward for future passive and additive-free flow assurance applications in the oil and gas arena.

## ASSOCIATED CONTENT

### Supporting Information

Details of cyclopentane adhesion measurements, schematic showing prevention of fluorine group reorientation in thinner pPFDA layer (10 nm), photograph of adhesion test apparatus, and video of hydrate formation. The Supporting Information is available free of charge on the ACS Publications website at DOI: 10.1021/acs.langmuir.5b00413.

## AUTHOR INFORMATION

### Corresponding Authors

*E-mail: kkg@mit.edu (K.K.G.).
*E-mail: gareth@mit.edu (G.H.M).

### Notes

The authors declare no competing financial interest.

## ACKNOWLEDGMENTS

The authors gratefully acknowledge support from the Chevron-MIT Energy Initiative program. The authors would like to thank Prof Kripa K. Varanasi and Srinivas Prasad Bengaluru Subramanyam for their assistance with the adhesion measurements.

## REFERENCES

(1) Sloan, E. D.; Koh, C. A. *Clathrate Hydrates of Natural Gases*; CRC Press: Boca Raton, FL, 2007.



DOI: 10.1021/acs.langmuir.5b00413
*Langmuir* 2015, 31, 6186−6196

(2) Dyadin, Y. A.; Bondaryuk, I. V.; Aladko, L. S. Stoichiometry of clathrates. *J. Struct. Chem.* **1995**, *36* (6), 995−1045.
(3) Bollavaram, P.; Devarakonda, S.; Selim, M. S.; Sloan, E. D. Growth kinetics of single crystal sII hydrates: Elimination of mass and heat transfer effects. *Ann. N. Y. Acad. Sci.* **2000**, *912*, 533−543.
(4) Wilson, P. W.; Lester, D.; Haymet, A. D. J. Heterogeneous nucleation of clathrates from supercooled tetrahydrofuran (THF)/water mixtures, and the effect of an added catalyst. *Chem. Eng. Sci.* **2005**, *60* (11), 2937−2941.
(5) Sum, A. K.; Koh, C. A.; Sloan, E. D. Clathrate Hydrates: From Laboratory Science to Engineering Practice. *Ind. Eng. Chem. Res.* **2009**, *48* (16), 7457−7465.
(6) Aman, Z. M.; Olcott, K.; Pfeiffer, K.; Sloan, E. D.; Sum, A. K.; Koh, C. A. Surfactant Adsorption and Interfacial Tension Investigations on Cyclopentane Hydrate. *Langmuir* **2013**, *29* (8), 2676−2682.
(7) Ecker, C.; Dvorkin, J.; Nur, A. Sediments with gas hydrates: Internal structure from seismic AVO. *Geophysics* **1998**, *63* (5), 1659−1669.
(8) Gbaruko, B. C.; Igwe, J. C.; Gbaruko, P. N.; Nwokeoma, R. C. Gas hydrates and clathrates: Flow assurance, environmental and economic perspectives and the Nigerian liquified natural gas project. *J. Pet. Sci. Eng.* **2007**, *56* (1−3), 192−198.
(9) Devarakonda, S.; Groysman, A.; Myerson, A. S. THF-water hydrate crystallization: an experimental investigation. *J. Cryst. Growth* **1999**, *204* (4), 525−538.
(10) Koh, C. A.; Westacott, R. E.; Zhang, W.; Hirachand, K.; Creek, J. L.; Soper, A. K. Mechanisms of gas hydrate formation and inhibition. *Fluid Phase Equilib.* **2002**, *194*, 143−151.
(11) Gao, S. Q. Hydrate Risk Management at High Watercuts with Anti-agglomerant Hydrate Inhibitors. *Energy Fuels* **2009**, *23*, 2118−2121.
(12) Smith, J. D.; Meuler, A. J.; Bralower, H. L.; Venkatesan, R.; Subramanian, S.; Cohen, R. E.; McKinley, G. H.; Varanasi, K. K. Hydrate-phobic surfaces: fundamental studies in clathrate hydrate adhesion reduction. *Phys. Chem. Chem. Phys.* **2012**, *14* (17), 6013−6020.
(13) Sojoudi, H.; McKinley, G. H.; Gleason, K. K. Linker-Free Grafting of Fluorinated Polymeric Cross-linked Network Bilayers for Durable Reduction of Ice Adhesion. *Mater. Horiz.* **2015**, *2* (1), 91−99.
(14) Coclite, A. M.; Howden, R. M.; Borrelli, D. C.; Petruczok, C. D.; Yang, R.; Yague, J. L.; Ugur, A.; Chen, N.; Lee, S.; Jo, W. J.; Liu, A. D.; Wang, X. X.; Gleason, K. K. 25th Anniversary Article: CVD Polymers: A New Paradigm for Surface Modification and Device Fabrication. *Adv. Mater.* **2013**, *25* (38), 5392−5422.
(15) Coclite, A. M.; Shi, Y. J.; Gleason, K. K. Grafted Crystalline Poly-Perfluoroacrylate Structures for Superhydrophobic and Oleophobic Functional Coatings. *Adv. Mater.* **2012**, *24* (33), 4534−4539.
(16) Ozaydin-Ince, G.; Coclite, A. M.; Gleason, K. K. CVD of polymeric thin films: applications in sensors, biotechnology, microelectronics/organic electronics, microfluidics, MEMS, composites and membranes. *Rep. Prog. Phys.* **2012**, *75* (1), No. 016501.
(17) Sojoudi, H.; Gleason, K. K.; McKinley, G. H. Designing Durable Vapor Deposited Surfaces for Reduced Hydrate Adhesion. *Adv. Mater. Interfaces* **2015**, DOI: 10.1002/admi.201500003.
(18) Aman, Z. M.; Brown, E. P.; Sloan, E. D.; Sum, A. K.; Koh, C. A. Interfacial mechanisms governing cyclopentane clathrate hydrate adhesion/cohesion. *Phys. Chem. Chem. Phys.* **2011**, *13* (44), 19796−19806.
(19) Aman, Z. M.; Joshi, S. E.; Sloan, E. D.; Sum, A. K.; Koh, C. A. Micromechanical cohesion force measurements to determine cyclopentane hydrate interfacial properties. *J. Colloid Interface Sci.* **2012**, *376*, 283−288.
(20) Aman, Z. M.; Leith, W. J.; Grasso, G. A.; Sloan, E. D.; Sum, A. K.; Koh, C. A. Adhesion Force between Cyclopentane Hydrate and Mineral Surfaces. *Langmuir* **2013**, *29* (50), 15551−15557.
(21) Subramanyam, S. B.; Rykaczewski, K.; Varanasi, K. K. Ice Adhesion on Lubricant-Impregnated Textured Surfaces. *Langmuir* **2013**, *29* (44), 13414−13418.
(22) Aspenes, G.; Dieker, L. E.; Aman, Z. M.; Hoiland, S.; Sum, A. K.; Koh, C. A.; Sloan, E. D. Adhesion force between cyclopentane hydrates and solid surface materials. *J. Colloid Interface Sci.* **2010**, *343* (2), 529−536.
(23) Dieker, L. E.; Aman, Z. M.; George, N. C.; Sum, A. K.; Sloan, E. D.; Koh, C. A. Micromechanical Adhesion Force Measurements between Hydrate Particles in Hydrocarbon Oils and Their Modifications. *Energy Fuels* **2009**, *23*, 5966−5971.
(24) Taylor, C. J.; Dieker, L. E.; Miller, K. T.; Koh, C. A.; Sloan, E. D. Micromechanical adhesion force measurements between tetrahydrofuran hydrate particles. *J. Colloid Interface Sci.* **2007**, *306* (2), 255−261.
(25) Yang, S. O.; Kleehammer, D. M.; Huo, Z. X.; Sloan, E. D.; Miller, K. T. Temperature dependence of particle-particle adherence forces in ice and clathrate hydrates. *J. Colloid Interface Sci.* **2004**, *277* (2), 335−341.
(26) Song, J. H.; Couzis, A.; Lee, J. W. Direct Measurements of Contact Force between Clathrate Hydrates and Water. *Langmuir* **2010**, *26* (12), 9187−9190.
(27) Song, J. H.; Couzis, A.; Lee, J. W. Investigation of Macroscopic Interfacial Dynamics between Clathrate Hydrates and Surfactant Solutions. *Langmuir* **2010**, *26* (23), 18119−18124.
(28) Karanjkar, P. U.; Lee, J. W.; Morris, J. F. Calorimetric investigation of cyclopentane hydrate formation in an emulsion. *Chem. Eng. Sci.* **2012**, *68* (1), 481−491.
(29) Karanjkar, P. U.; Lee, J. W.; Morris, J. F. Surfactant Effects on Hydrate Crystallization at the Water-Oil Interface: Hollow-Conical Crystals. *Cryst. Growth Des.* **2012**, *12* (8), 3817−3824.
(30) Zylyftari, G.; Lee, J. W.; Morris, J. F. Salt effects on thermodynamic and rheological properties of hydrate forming emulsions. *Chem. Eng. Sci.* **2013**, *95*, 148−160.
(31) Nakajima, M.; Ohmura, R.; Mori, Y. H. Clathrate Hydrate Formation from Cyclopentane-in-Water Emulsions. *Ind. Eng. Chem. Res.* **2008**, *47* (22), 8933−8939.
(32) Sefidroodi, H.; Abrahamsen, E.; Kelland, M. A. Investigation into the strength and source of the memory effect for cyclopentane hydrate. *Chem. Eng. Sci.* **2013**, *87*, 133−140.
(33) Brown, C. J.; Ni, X. Evaluation of rate of cyclopentane hydrate formation in an oscillatory baffled column using laser induced fluorescence and energy balance. *Chem. Eng. J.* **2010**, *157* (1), 131−139.
(34) Coclite, A. M.; Shi, Y. J.; Gleason, K. K. Controlling the Degree of Crystallinity and Preferred Crystallographic Orientation in Poly-Perfluorodecylacrylate Thin Films by Initiated Chemical Vapor Deposition. *Adv. Funct. Mater.* **2012**, *22* (10), 2167−2176.
(35) Smith, G. W.; Sorg, L. V. The measurement of boundary tension by the pendant-drop method. I The aliphatic alcohols. *J. Phys. Chem.* **1941**, *45* (4), 671−681.
(36) Korhonen, J. T.; Huhtamaki, T.; Ikkala, O.; Ras, R. H. A. Reliable Measurement of the Receding Contact Angle. *Langmuir* **2013**, *29* (12), 3858−3863.
(37) Meuler, A. J.; Smith, J. D.; Varanasi, K. K.; Mabry, J. M.; McKinley, G. H.; Cohen, R. E. Relationships between Water Wettability and Ice Adhesion. *ACS Appl. Mater. Interfaces* **2010**, *2* (11), 3100−3110.
(38) Ozaydin-Ince, G.; Gleason, K. K. Transition between kinetic and mass transfer regimes in the initiated chemical vapor deposition from ethylene glycol diacrylate. *J. Vac. Sci. Technol. A* **2009**, *27* (5), 1135−1143.
(39) Yang, R.; Buonassisi, T.; Gleason, K. K. Organic Vapor Passivation of Silicon at Room Temperature. *Adv. Mater.* **2013**, *25* (14), 2078−2083.
(40) Petruczok, C. D.; Yang, R.; Gleason, K. K. Controllable Cross-Linking of Vapor-Deposited Polymer Thin Films and Impact on Material Properties. *Macromolecules* **2013**, *46* (5), 1832−1840.
(41) Yague, J. L.; Gleason, K. K. Enhanced Cross-Linked Density by Annealing on Fluorinated Polymers Synthesized via Initiated Chemical Vapor Deposition To Prevent Surface Reconstruction. *Macromolecules* **2013**, *46* (16), 6548−6554.





DOI: 10.1021/acs.langmuir.5b00413
*Langmuir* 2015, 31, 6186−6196

(42) Zhang, Y. F.; Debenedetti, P. G.; Prud'homme, R. K.; Pethica, B. A. Differential scanning calorimetry studies of clathrate hydrate formation. *J. Phys. Chem. B* **2004**, *108* (43), 16717−16722.
(43) Fouconnier, B.; Komunjer, L.; Ollivon, M.; Lesieur, P.; Keller, G.; Clausse, D. Study of CCl(3)F hydrate formation and dissociation in W/O emulsion by differential scanning calorimetry and X-ray diffraction. *Fluid Phase Equilib.* **2006**, *250* (1−2), 76−82.
(44) Clausse, D. Differential thermal analysis, differential scanning calorimetry, and emulsions. *J. Therm. Anal. Calorim.* **2010**, *101* (3), 1071−1077.
(45) Feistel, R.; Wagner, W. A new equation of state for H2O ice Ih. *J. Phys. Chem. Ref. Data* **2006**, *35* (2), 1021−1047.
(46) Hennig, A.; Grundke, K.; Frenzel, R.; Stamm, M. Ultra-hydrophobic surfaces: Relation between roughness and contact angle hysteresis. *Tenside, Surfactants, Deterg.* **2002**, *39* (6), 243−246.
(47) Corak, D.; Barth, T.; Hoiland, S.; Skodvin, T.; Larsen, R.; Skjetne, T. Effect of subcooling and amount of hydrate former on formation of cyclopentane hydrates in brine. *Desalination* **2011**, *278* (1−3), 268−274.
(48) De Souza, E. J.; Gao, L. C.; McCarthy, T. J.; Arzt, E.; Crosby, A. J. Effect of contact angle hysteresis on the measurement of capillary forces. *Langmuir* **2008**, *24* (4), 1391−1396.
(49) Gao, L. C.; McCarthy, T. J. Teflon is hydrophilic. Comments on definitions of hydrophobic, shear versus tensile hydrophobicity, and wettability characterization. *Langmuir* **2008**, *24* (17), 9183−9188.
(50) Gao, L. C.; McCarthy, T. J. Wetting 101 degrees. *Langmuir* **2009**, *25* (24), 14105−14115.
(51) Kim, P.; Wong, T. S.; Alvarenga, J.; Kreder, M. J.; Adorno-Martinez, W. E.; Aizenberg, J. Liquid-Infused Nanostructured Surfaces with Extreme Anti-Ice and Anti-Frost Performance. *ACS Nano* **2012**, *6* (8), 6569−6577.

## ■ NOTE ADDED AFTER ASAP PUBLICATION

This paper was published on the Web on May 26, 2015, with errors in the reference numbering. The corrected version was reposted on May 28, 2015.





DOI: 10.1021/acs.langmuir.5b00413
*Langmuir* 2015, 31, 6186−6196